# EXPLORATION OF THE NUCLEATION PATHWAY FOR SUPRAMOLECULAR FIBERS

Phu K. Tang[1,2], Prabir Khatua[1], Vincenzo Carnevale[3], Sharon M. Loverde[1,2,4]

[1] *Department of Chemistry, College of Staten Island, The City University of New York, 2800 Victory Boulevard, Staten Island, New York 10314, United States*

[2] *Ph.D. Program in Biochemistry, The Graduate Center of the City University of New York, New York, New York 10016, United States*

[3] *Institute for Computational Molecular Science, Temple University, Philadelphia, PA 19122*

[4] *Ph.D. Program in Chemistry and Physics, The Graduate Center of the City University of New York, New York, New York 10016, United States*

**ABSTRACT:** The pathway for supramolecular fiber formation is coupled to the underlying order of the self-assembling molecules. Here, we report on atomistic molecular dynamics simulations to characterize the initial stages of the self-assembly of a model drug amphiphile in an aqueous solution. We perform two-dimensional metadynamics calculations to characterize the assembly space of this model drug amphiphile—Tubustecan, TT1. TT1 is composed of the hydrophobic anti-cancer drug, Camptothecin (CPT), conjugated to a hydrophilic polyethylene glycol (PEG) chain. We find that the aromatic stacking of CPT drives the formation of a higher-density liquid droplet. This droplet elongates and can form a higher-ordered supramolecular assembly upon reorganizing and forming an interface and additional aromatic stacking of the drugs. We show that novel reaction coordinates tailored to this class of molecules are essential in capturing varying degrees of the underlying degree of molecular order upon assembly. This approach can be refined and extended to characterize the supramolecular assembly pathway of other molecules containing aromatic compounds.

## INTRODUCTION

Supramolecular polymers have diverse applications in bio- and electronic materials[1]. The dominant intermolecular forces in these systems, determined by the solvation environment, set the path for a thermodynamically stable or a kinetically trapped intermediate[2]. While filamentous assemblies in solution are frequently driven by hydrogen bonding and amyloid formation[3-4], peptide or polymer-conjugated aromatic molecules suggest another path to one-dimensional fiber formation[5-7]. Indeed, peptide-conjugated aromatic molecules possess numerous applications[8-9]. Kinetic pathways for fiber formation involve nucleation, elongation, and secondary nucleation[4]. The pathway to metastable aggregates can be further delineated[10]. Minimalistic models that describe dynamic equilibrium have been reported[11]. Machine learning models can describe the degree of molecular order[12] or be used to screen many molecular sequences and topologies[13-14].

Molecular simulations to explore the assembly pathway of peptide-based amphiphiles have addressed the multi-step aggregation process[15]. For peptides conjugated to aromatics, it is shown that aromatic stacking drives the early stages of the self-assembly process[16]. Coarse-grained (CG) simulations have that drug amphiphiles (DAs) form a high-density liquid droplet that is stable for microsecond timescales[17]. As applied to the self-assembly of amphiphilic systems, free energy methods are evolving as a toolset to unveil key rational design rules. Quantitative structure-property relationship (QSPR) models and free energy methods have established design rules for assembling conjugated aromatic peptides with optoelectronic functionality[18]. Screening the strength of intermolecular interactions using metadynamics has proven to be a novel approach to investigate the assembly pathway for various combinations of oppositely charged peptides[19]. Here we report on atomistic molecular dynamics (MD) simulations that utilize advanced sampling methods (metadynamics[20]) to characterize the initial energy landscape for the assembly of model drug amphiphiles[7]. This computational approach can be applied to explore the self-assembly pathway of these model DAs and is based on the underlying molecular chemistry. This approach can also be extended to characterize the initial pathway for the assembly of molecular amphiphiles, whereas intermolecular forces may be specific and directional.

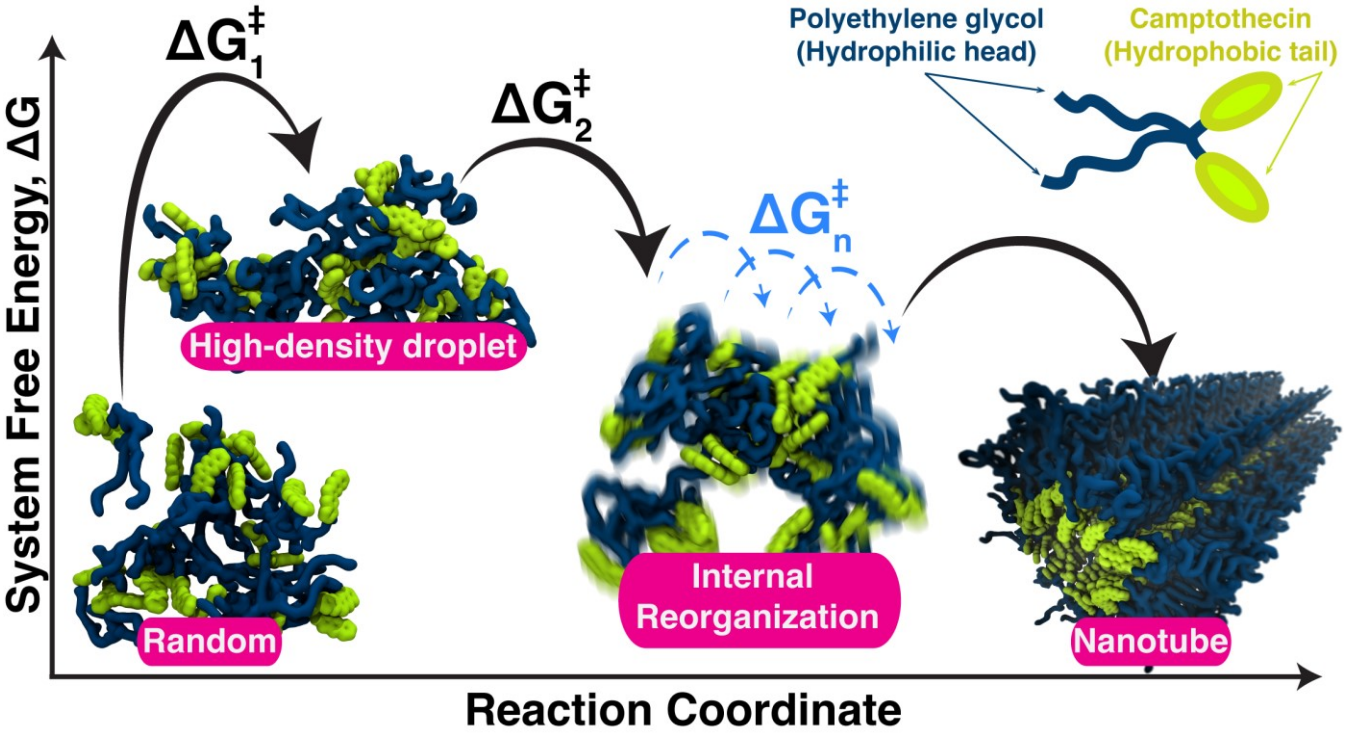


Figure 1. A proposed nucleation mechanism of a drug amphiphile composed of a hydrophilic head and hydrophobic tail. We plot the proposed system free energy, ΔG, along the assembly pathway projected on an arbitrary reaction coordinate. The drug amphiphile TT1 self-assembles from a random to a high-density droplet, followed by internal reorganization. More intermediates are sampled during reorganization, depicted as light-blued arrows until the final state (nanotube) is reached. The top right corner shows the schematic representation of TT1 with Camptothecin drugs highlighted in lime, and the PEG headgroup is highlighted in dark blue.

Herein, we propose that fluctuations in density near a critical radius facilitate the formation of high-density liquid-like droplets, also known as condensates. Then, internal reorganization within these high-density droplets further lowers the energy barrier to a more ordered fiber or nanotube. However, the amphiphile molecular structure contributes to the free energy and introduces the possibility of micellization. Notably, the formation of a high-density liquid-like droplet has been shown to drive the formation of micelles at the liquid-liquid interface for block copolymer micelles. These micelles can fuse and form higher-order vesicle assemblies[21]. *Tirrell et al.* have also reported the formation of transient spherical micelles that form on the pathway to the formation of worm-like micelles[22]. Fibrous assembly has also been coupled to liquid-liquid phase separation (LLPS) for short amphiphilic peptide sequences[23]. One-dimensional assemblies can be nanotubes with hollow cores[24-25] or display varying chirality such as twisted ribbons[26], etc. The pathway to fibril formation may entail thermodynamically and kinetically favored aggregates[27]. Here, we propose a mechanism whereby high-density droplets, also known as condensates, promote the formation of a more ordered supramolecular assembly upon internal rearrangement of the amphiphiles. Forming a PEG-drug interface and uni-directional stacking of the CPT drugs drives internal rearrangement.

This article explores the nucleation pathway for drug amphiphiles (DAs) schematically shown in microfilaments or nanotubes. These structures are designed as drug delivery vehicles.[6-7, 28] For example, Tubustecan 1 (TT1) is a prototype DA that self-assembles into nanotubes with a diameter in the range of ~ 10 nm in solutions at concentrations (~ 200-800 μm), which is higher than the critical micelle concentration (CMC), as shown in **Figure S6**.[7] The chemical structure of TT1 can be found in **Figure S1**. TT1 delivers Camptothecin (CPT) analogs that can act as potent anti-cancer therapeutics.[7] As shown in **Figure** 1, a TT1 consists of two CPTs chemically linked to two polyethylene glycol (PEG) chains via reducible disulfide linkers. *In vitro* data shows that TT1 yields the best results in the maximum tolerated dose and survival chance compared to additional prototypes. Spectroscopic analysis of the TT1 nanotubes via circular dichroism (CD) reveals that the aromatic rings from CPTs are structurally ordered at the core of the nanotube.[7] While experimental methods such as CD spectra or SAXS can inform on the degree of order in such assemblies, these methods report the average static properties at late assembly time scales. The initial stages of self-assembly are at microseconds to seconds time scales. For example, *Loverde et al.* use MD simulations to characterize the interactions of a similar DA system with a model membrane.[29] More studies on these DAs using molecular dynamics (MD) simulations can be found elsewhere.[6, 15-16, 28, 30]

## RESULTS AND DISCUSSION

These TT1 molecules, model amphiphilic molecules, display strong aromatic interactions that drive self-assembly. As

mentioned, we want to explore the DA's assembly pathway using conventional MD methods. However, nucleation is a rare event entailing enhanced sampling methods[31-35] in molecular dynamics, such as reaction-coordinate-based (umbrella sampling[36-38], metadynamics) or path-based sampling[31, 39-42] based methods. Specifically, we use metadynamics[20, 43-45] to drive the self-assembly of the CPTs via π-π stacking, which is known to be driving the self-assembly of similar DAs with these conjugated CPT drugs.[7] Here, we reduce the complexity of the whole conformational landscape to two reaction coordinates in metadynamics: $S_L$, the total coordination of the largest cluster,[45-46], and the relative shape anisotropy $\kappa^2$. An overview of metadynamics and the chosen reaction coordinates is given in the **SI.** We perform four sets of MD simulations, as summarized in **Table 1.**

Table 1. **Summary of simulated systems.**

| MD Method | Conventional | | Metadynamics | |
|---|---|---|---|---|
| System | CPT-Only | I | II | III |
| Atoms | 72,582 | 27,888 | | |
| Box Size (Å) | 95 × 92 × 91 | 94 × 101 × 94 | | |
| Concentration | 50 mM | | | |
| Temperature | 300 K | | | |
| Simulated Time | 100 ns | | | |
| Reaction Coordinate | N/A | | $S_L$ | $S_L$ & $\kappa^2$ |
| σ | | | 10 | 10 & 0.1 |
| W, kcal/mol | | | 2 | 1.5 |
| Deposited Frequency τ, step | | | 100 | 500 |

Next, we focus on how adding the PEG headgroup modulates the nucleation pathway of these CPTs, allowing for micellization. Hybrid experimental and computational approaches have much potential to explore the self-assembly pathway for supramolecular assemblies. For instance, cryo-TEM and coarse-grained simulations reveal that amphiphilic Janus dendrimers with varying degrees of hydrophobicity form many shapes, such as cubic (or cubosomes), disk-like, tubular, and helical ribbons.[47] Here, we show that the PEG headgroup alters the elongation trend of free CPT molecules, which tend to form rod-, needle-[48], sheet-like[49] shaped nanocrystals under appropriate solvent conditions. To characterize the degree of π-π stacking, we also define a stacking index $\Xi_\pi$. For example, higher values of $\Xi_\pi$ indicate a greater degree of stacking, potentially suggesting an ordered arrangement of CPTs. Additionally, acylindricity *c*, calculated from the principal moments of the gyration tensor, can quantify the similarity of an aggregate shape to a cylinder. More details can be found in the **Supporting Information (SI)**.

Visually investigating the MD trajectories of the CPT-Only system and system I, both simulated with conventional MD, shows that the PEG headgroup interrupts the intrinsic stacking of the CPTs. We calculate the normalized radial distribution function (g(r)) of the distance between the center of mass of the CPT modules in all simulated systems: the CPT-Only, systems I, II, and III, as shown in **Figure 2.**

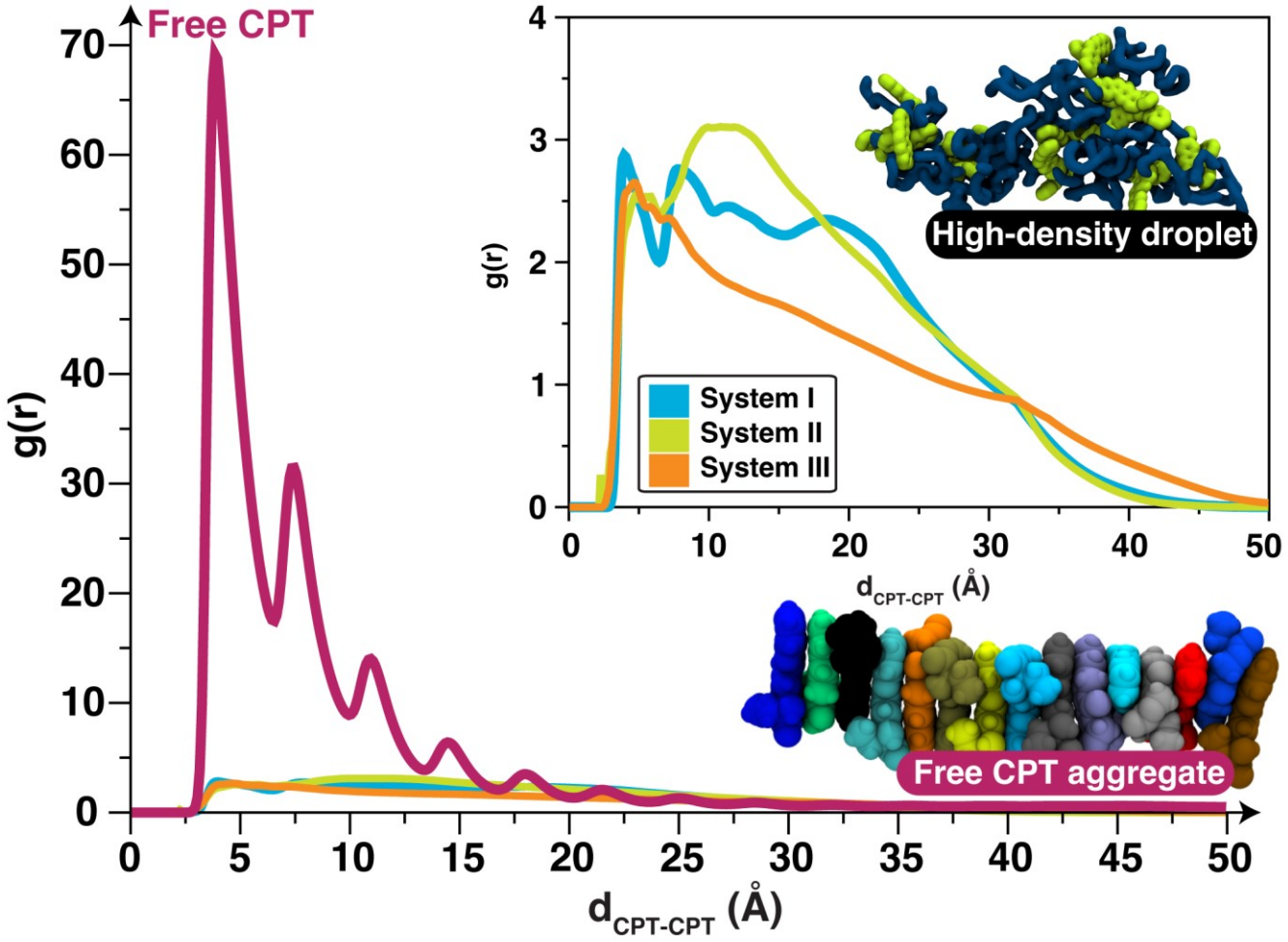


Figure 2. Normalized radial distribution function g(r) of the distance between the center of mass of CPTs. The inset shows the g(r) of the distance between the center of mass of CPTs for systems I, II, and III. The magenta line is the g(r) for the free CPT system. Blue, green, and orange lines are the g(r) 's for system I (conventional MD), system II (1-D metadynamics), and system III (2-D metadynamics).

---

In **Figure 2**, the normalized g(r) of the CPT-Only system shows that its first peak is significantly strong, while that of system I exhibits a relatively weak peak. The magnitude of the first peak and g(r) shape suggests that the CPT-Only system tends to form an elongated chain of stacked CPTs or a 'Free CPT aggregate.' Attaching a PEG headgroup to the CPTs (system I) promotes the formation of a more liquid-like structure or a 'High-density droplet,' as shown in the snapshots of **Figure 2**. This ' High-density droplet' resembles the transient spherical micelle droplets reported by *Tirrell et al.* on the path to more elongated worm-like micelles[22]. For the case of these drug amphiphiles, we show that these droplets allow for the movement of the drug inwards towards the center, promoting aromatic stacking of the drugs. At the same time, increased stacking drives the stretching of the droplet in one direction.

When metadynamics is applied to TT1 in systems II and III, the g(r) shift strongly suggests that the method shifts the local degree of ordered CPTs, as shown in **Figure 2** inset. Indeed, the g(r) loses the multiple peaks but the main peak shifts to larger distances. We next calculate the normalized g(r) and the potential of mean force (PMF), $W(r) = -k_B T \ln g(r)$, for particular conformations that exhibit the highest coordination number between CPTs. **Figure S3 A** shows the normalized g(r) profiles for these particular conformations. The PMF shows that these selected conformations exhibit a lower energy state. This demonstrates that this approach allows the exploration of lower energy states along the reaction coordinate that are challenging to sample with conventional MD.

We note that multiple parameters regarding this approach can be further refined. The first reaction coordinate, the total coordination of the largest cluster, $S_L$, has a cutoff. We initially chose the cutoff based on previous works by our laboratory in which we determined the lowest energy conformation between two CPTs with multiple walker metadynamics.[16] The cutoff should be adjusted if this approach were applied to sample the coordination between

differently shaped amphiphiles with the lowest energy conformation at a larger or smaller distance. For example, the packing and interactions between paclitaxel are solvent and concentration-dependent[50] with an alternating head-to-tail packing described by Mastropaolo et al. [51]. As applied to paclitaxel, the cutoff for this approach would need to be much higher.

We next compare the clustering trends between all systems with respect to the CPT-Only system. We calculate the distribution of stacking fraction $\Xi_\pi$, total coordination of the largest cluster $S_L$, acylindricity c, and shape anisotropy $\kappa^2$ over the first and last 10% of the simulation time. In the CPT-Only system, $\Xi_\pi$ is significantly higher than in the other simulations, as shown in **Figure 3 A**. At the end of the 100 ns simulation, the stacking fraction has greatly increased in the CPT-Only system. This is expected, as CPT is known to form stacked crystals[48]. At the end of the simulations, there is little change in stacking fraction for systems I, II, and III. This little difference in the $\Xi_\pi$, suggests a high energy barrier. At the same time, **Figure 3 B** shows that the distribution of $S_L$ in systems II and III peaks at higher values than the other simulations. This indicates that metadynamics can better sample the free energy landscape of TT1 as the $S_L$ for systems II and III are sampled over a broader range. In other words, the CPT tails aggregate more with metadynamics, but the π-π stacking is limited. **Figure 3 C and D** demonstrate that the CPT-Only simulation displays more acylindricity and more significant variation in shape anisotropy than TT1s. In **Figure 3 C**, TT1s are more prone to forming cylindrical shapes than the CPT-only system. We speculate that the PEG headgroup promotes cylindrical shape formation for TT1 by modulating the π-π stacking of the CPT tails; whether this results in the ultimate nanotube requires more sophisticated models and additional experimental data. Taken together, **Figure 2** and **Figure 3** demonstrate that adding the PEG headgroup impedes the stacking of CPTs.

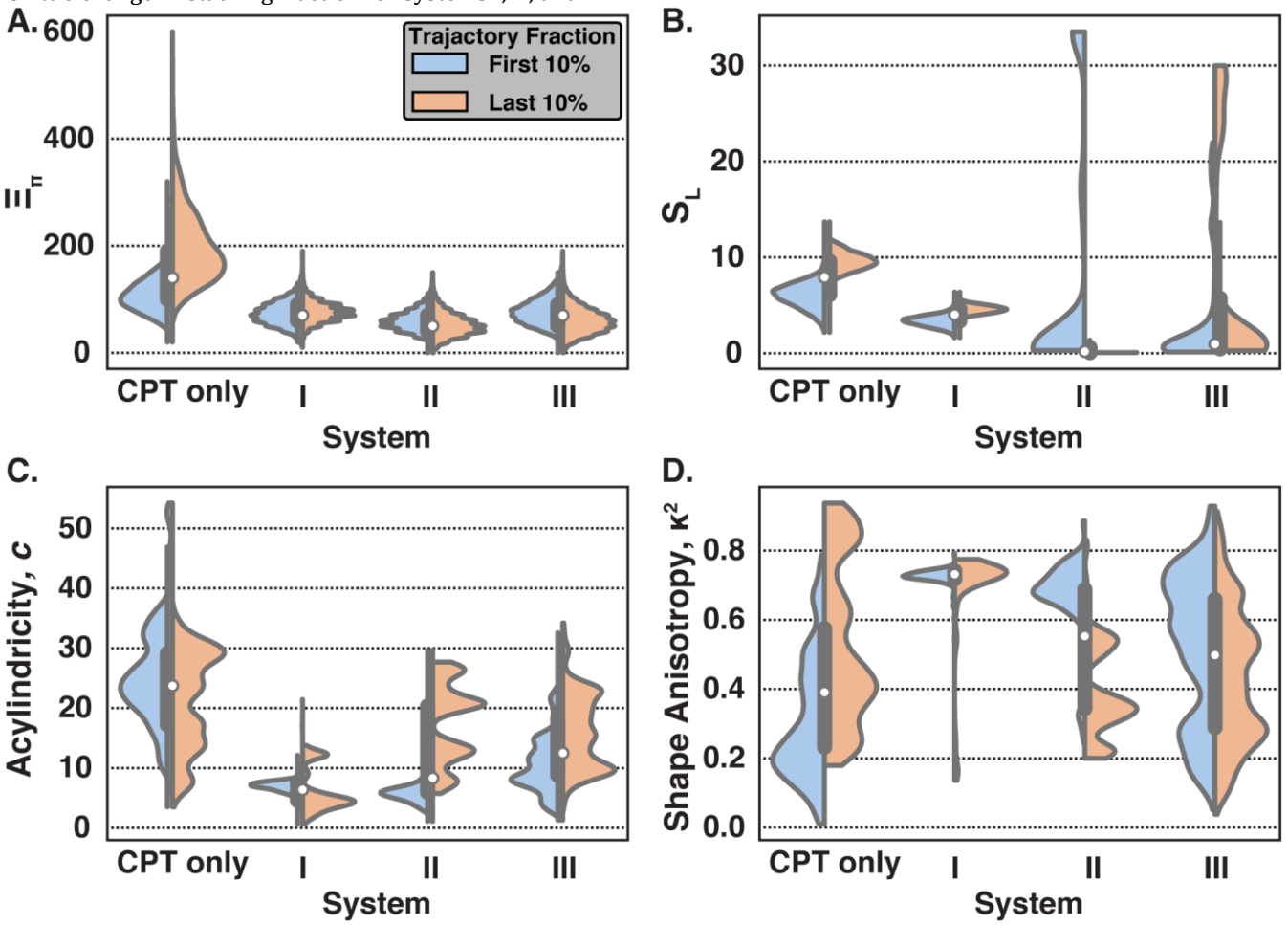


Figure 3. Clustering trends of all systems at the first 10% (blue) and the last 10% (orange) of simulation time. Systems 0 and I are simulated for 100 ns, while systems II and III were simulated for 50 ns. **(A)** Stacking Index Ξπ **(B)** $S_L$ **(C)** Acylindricity c **(D)** Shape Anisotropy $\kappa^2$. The black boxes represent the distribution quartiles, with the white circles being the average.

---

Next, we compare the 2D PMF profiles for conventional MD and metadynamics. **Figure S4 A—C** shows that conventional MD is sufficient to sample the CPT-Only system. The 2D PMF profiles set a baseline for comparing systems I, II, and III. A closer look at the 2D PMF profiles of system I, in **Figure S2 A—C**, reveal that, for 100 ns, the $S_L$ values of TT1 are indeed very stable since the minimum peaks are significant and have minimum free energies of about 0.6 kcal/mol.

Thus, it is unreasonable to use conventional MD simulations as high activation energy can kinetically trap TT1s in a local energy basin. As such, metadynamics is an enhanced sampling method to quickly sample complex reaction coordinates, such as $S_L$ and $\kappa^2$, to characterize the assembly of TT1. In **Figure 4,** all $S_L$ reach a higher maximum value due to metadynamics, which implies that the method allows the formation of a more coordinated liquid droplet than the CPT-only simulations. **Figure 4A** exhibits multiple clearly defined peaks. The multiple peaks indicate multiple states. The two higher peaks higher in $S_L$ are due to two different conformations of liquid-like droplets. **Figure 4B** also exhibits its multiple peaks. Four peaks (B1 to B4) are in a low acylindricity range (more cylindrical). Notably, the CPTs localize closer to the COM of the droplet for these conformations with low acylindricity. In other words, the more inward positioning of the CPTs is related to the cylindrical propensity of the TT1s. We hypothesize that as the CPTs move toward the center of the droplet, they stretch the droplet due to increased stacking. We suggest that the π-π stacking between the aromatic rings may drive the flip of the DA inwards. While the CD spectrum shows the CPT packing at the core of the nanotube, it isn't easy to assess the time-dependent dynamics of tube formation from this reported data.[7]

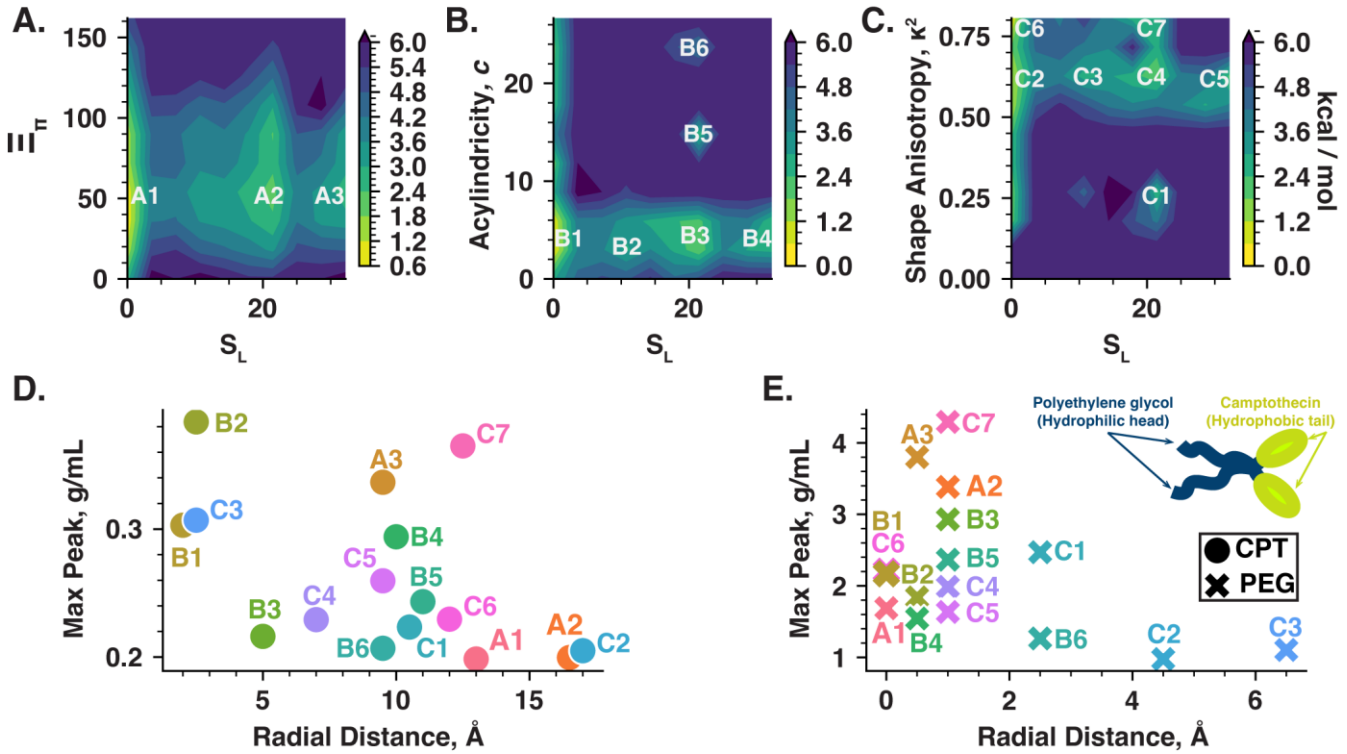


Figure 4. Characteristics of System II (1D Metadynamics). 2D PMF profiles between $S_L$ and **(A)** Stacking Index $\Xi_\pi$ **(B)** Acylindricity c **(C)** Shape Anisotropy $\kappa^2$. **(D)** The radial density of CPT tails **(E)** The radial density of PEG headgroup. Only the maximum signal from each highlighted peak's radial mass density profile is plotted. The circle represents the drug density, and the cross represents the PEG headgroup density.

---

**Figure 4C** also exhibits multiple peaks, some of which have a very high shape anisotropy. This is consistent with the previous hypothesis that some droplets stretch as the CPTs move inwards and stack, and the stretching is correlated with higher anisotropy in the droplet shape. Figure 4 C shows that C7 (0.36 g/mL) has the highest $S_L$ and $\kappa^2$. This is an example of a droplet with very high stacking and shape anisotropy.

One possible explanation is that when the ordered CPTs are dense enough and reach a particular value of $\kappa^2$, the outward CPTs will move inwards to transform to the next state. Additional experimental and theoretical studies can verify this movement. Attempting to pre-assemble a nanotube of TT1 with inward CPT tails, we follow the method described in *Loverde et al.* [16]. We find spontaneous breaking down of the pre-assembled TT1 nanotube into micelles after 20 ns (as shown in **Figure S7**). This is expected as we did not consider π-π stacking in the initial conditions of the tube. Thus, in future studies, we hypothesize that additional parameters, such as $S_L$ and $\kappa^2$, must be considered to sample the assembly pathway better.

To track the internal density of the liquid droplets formed with either bare CPTs or TT1s, we calculate radial mass density profiles for each identified basin on 2D PMF profiles of all systems. We only plot the maximum values from the radial mass density profiles for clarification. In **Figure S4 D—E**, bare CPTs stack well as their radial density profiles converge to the center. With an additional PEG headgroup, the

peaks of the CPT in radial density profiles are further away from the droplet's center of mass (COM), as shown in **Figure S2 D—E**. We hypothesize that the CPTs stay between the PEG headgroup and the water to minimize the surface tension with these short PEG headgroups.

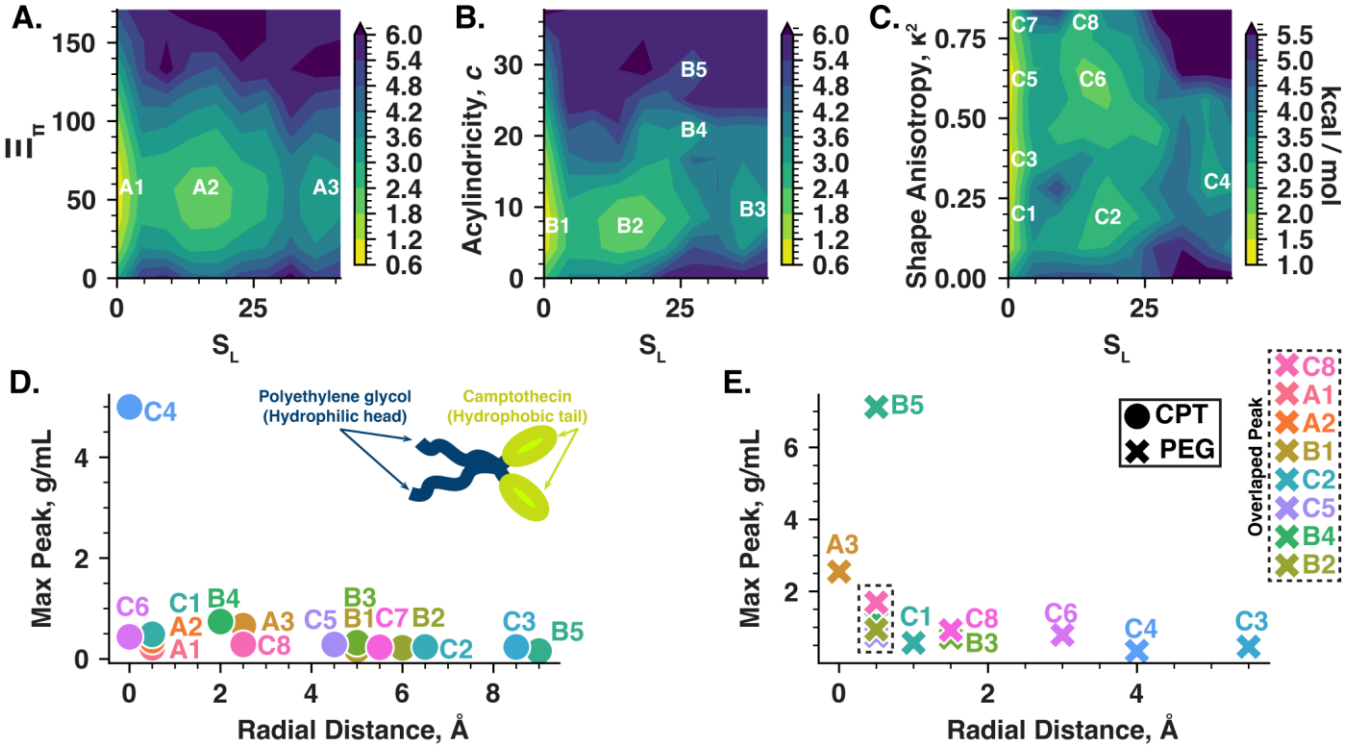


Figure 5. Characteristics of System III (2D Metadynamics). 2D PMF profiles between $S_L$ and **(A)** Stacking Index $\Xi_\pi$ **(B)** Acylindricity c **(C)** Shape Anisotropy $\kappa^2$. **(D)** The radial density of CPT tails **(E)** The radial density of PEG headgroup. Only the maximum signal from each highlighted peak's radial mass density profile is plotted. The circle represents the drug density, and the cross represents the PEG headgroup density.

---

To improve the sampling of droplet shape, we choose to apply 2D metadynamics. We apply metadynamics to both $S_L$ and $\kappa^2$ (system III). The 2D PMF profiles are shown in **Figure 5 A—C**. All peaks appear to broaden. For example, in **Figure 5 A**, the 2D PMF profile of $\Xi_\pi$ and $S_L$ appears to be shifted from a vertical peak, A2, to a more spherical peak at a similar $S_L$ range. Indeed, we find an increased sampling of all three reaction coordinates: $S_L$, $\kappa^2$, and c. In all three PMFs, additional states are sampled neighboring the original peaks. Interestingly, in **Figure 5 C,** an additional peak, labeled C4, with the highest density appears. C4 represents a highly compact cluster ($S_L$ = 30) with the highest mass density (5.0 g/mL). The CPTs in C4 also approach the COM of the cluster while its PEG headgroup is outwards, shown in **Figure 5 D** and **E**. This suggests the formation of a high-density liquid droplet during this course of the simulation. Previously, we have found the formation of a high-density liquid droplet using coarse-grained molecular dynamics for a slightly different molecular structure of the amphiphile[17]. Furthermore, the shift in drug density inwards is consistent with the hypothesis derived from **Figure 2**. The drug moves inwards, thus promoting aromatic stacking and stretching of the droplet.

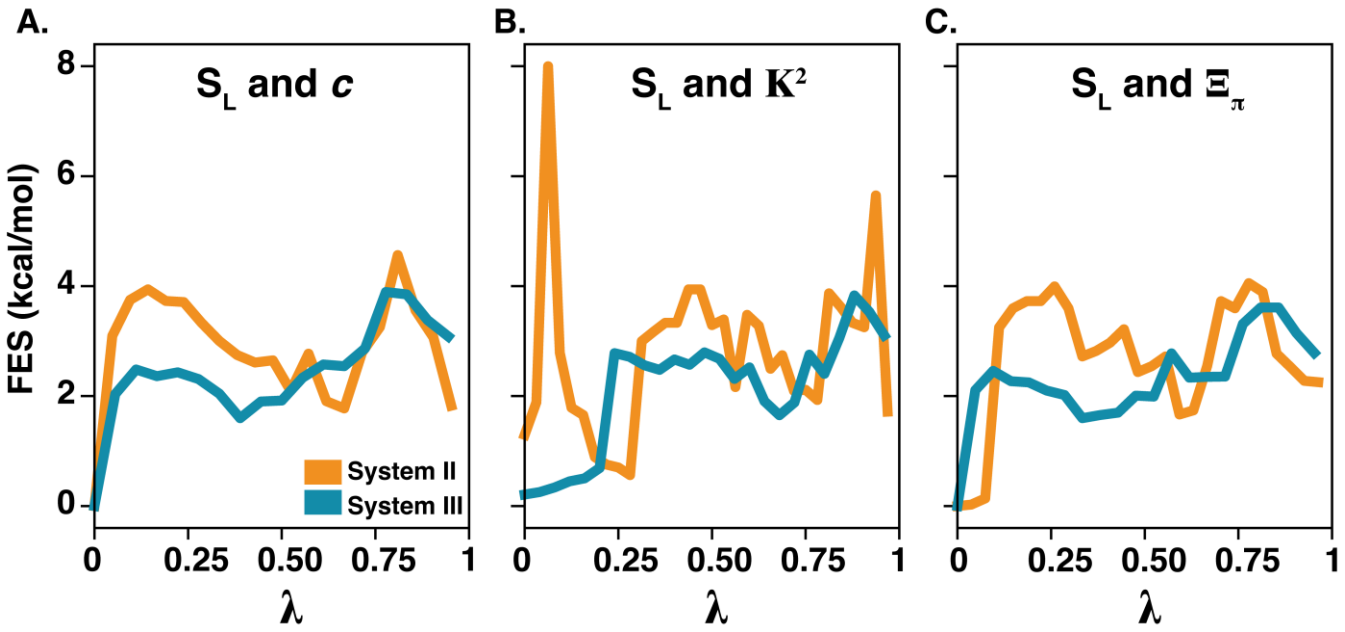


Figure 6. 1D free energy profiles are calculated from the 2D free energy profiles of 1D and 2D metadynamics for **(A)** $S_L$ and Acylindricity *c* **(B)** $S_L$ and Shape Anisotropy κ2 **(C)** $S_L$ and Stacking Index $\Xi_\pi$.

Assessing the convergence of these simulations is extraordinarily challenging due to the multiple dimensions of existing reaction coordinates. We show that the free energy profiles of the 1D metadynamics (system II) are qualitatively converged by performing annealing simulations (see a detailed method in **SI**). We obtain a different Boltzmann distribution of TT1's initial configurations before running metadynamics with identical parameters used in system II. The free energy profiles of the two replicates are similar to the ones in **Figure 4**, as shown in **Figure S5.**

We next compare the results of the three sets of PMFs by generalizing them to a 1D pathway. We extrapolate 1D profiles from the 2D profiles in **Figure 4** (1D metadynamics) and **Figure 5** (2D metadynamics) with **λ** as a hyper-reaction coordinate. **λ** describes the configurational space of the TT1 aggregates from low $S_L$ (0) to high $S_L$ (1). Indeed, all three 1D free energy profiles in **Figure 6** display an energy barrier followed by a metastable minimum and a secondary barrier for Systems II and III. Thus, these results suggest that kinetic models that contain both primary and secondary nucleation/elongation may support the initial stages of the self-assembly of these amphiphiles. As shown in **Figure 6,** system III, compared to system II, shows a reduction in the primary energy barrier. For example, **Figure 6 B** shows a significant reduction in the energy barrier from 8 kcal/mol to ~0.7 kcal/mol at the beginning of clustering (low $S_L$). Thus, system III (with two reaction coordinates) extensively explores the free energy landscape for SL and k2 in **Figure 5 C.** Again, we want to emphasize the importance and the possibilities of using free energy calculation methods, such as metadynamics, with reasonable reaction coordinates, which can explore complex free energy landscapes of these aromatic-conjugated amphiphiles.

A more thorough understanding of the self-assembly process is necessary to design synthetic biomaterials. There are numerous applications of supramolecular assemblies in medicine and energy, but our understanding of how these molecules reach their final assembled state is still evolving. This article attempts to elucidate the initial stages of the self-assembly pathway of TT1, a model prodrug, using advanced free energy methods in MD simulations. Our data suggest that TT1 follows a complex pathway whereby liquid-like droplets or condensates form and elongate. These elongated droplets allow the rearrangement of these amphiphiles and further stacking of the aromatic drug. We suggest several reactions coordinate to characterize the free energy landscape of these amphiphiles, including the acylindricity, the stacking fraction, the shape anisotropy, and the total coordination of the largest cluster. Herein, we utilize advanced sampling methods in molecular dynamics to outline a mechanism for assembling these novel drug amphiphiles. We note that a complete characterization of the phase diagram and the assembly pathway for the assembly of these amphiphiles will entail more extensive simulations over a range of concentrations both near and above the critical micelle concentration. In combination with the order parameters, as defined above, to characterize preliminary aggregates in the assembly pathway, different reaction coordinates can be defined to better sample the polymer shape and promote the formation of a more robust interface between polymer and drug. Additional advanced methods such as CG[17] and ML[12, 18], active learning, and cheminformatics methods may be combined with the computational methodology outlined herein to further characterize the energy landscape of model amphiphiles.

## ASSOCIATED CONTENT

## DATA AVAILABILITY STATEMENT

The data underlying this study are openly available in the GitHub repository named TT1 at https://github.com/phu91/TT1.

### Supporting Information

The Supporting Information is available free of charge on the ACS Publications website. Detailed simulation methods, a summary of the simulated systems, initial conformations of DAs, and definitions of all order parameters are given in the SI.

## AUTHOR INFORMATION

### Corresponding Author

*sharon.loverde@csi.cuny.edu **Sharon Loverde**

## ACKNOWLEDGMENT

S.M.L. acknowledges support from the NIH (R15EB020343-01A1). In addition, this research was supported, in part, by the NSF through grant 1506937. S.M.L. also acknowledges start-up funding from the College of Staten Island and the City University of New York.

## ABBREVIATIONS

TT1 Tubustecan 1; CPT Camptothecin; CNT classical nucleation theory; TSM two-step mechanism; DA drug-peptide amphiphile; CMC critical micelle concentration; CD circular dichroism; MD molecular dynamics; COM center of mass.

## REFERENCE

1. Aida, T.; Meijer, E. W.; Stupp, S. I., Functional Supramolecular Polymers. *Science* **2012,** *335* (6070), 813-817.
2. Tantakitti, F.; Boekhoven, J.; Wang, X.; Kazantsev, R. V.; Yu, T.; Li, J. H.; Zhuang, E.; Zandi, R.; Ortony, J. H.; Newcomb, C. J.; Palmer, L. C.; Shekhawat, G. S.; de la Cruz, M. O.; Schatz, G. C.; Stupp, S. I., Energy landscapes and functions of supramolecular systems. *Nature Materials* **2016,** *15* (4), 469-+.
3. Knowles, T. P. J.; Waudby, C. A.; Devlin, G. L.; Cohen, S. I. A.; Aguzzi, A.; Vendruscolo, M.; Terentjev, E. M.; Welland, M. E.; Dobson, C. M., An Analytical Solution to the Kinetics of Breakable Filament Assembly. *Science* **2009,** *326* (5959), 1533-1537.
4. Zimmermann, M. R.; Bera, S. C.; Meisl, G.; Dasadhikari, S.; Ghosh, S.; Linse, S.; Garai, K.; Knowles, T. P. J., Mechanism of Secondary Nucleation at the Single Fibril Level from Direct Observations of A beta 42 Aggregation. *Journal of the American Chemical Society* **2021,** *143* (40), 16621-16629.
5. Sis, M. J.; Ye, Z.; La Costa, K.; Webber, M. J., Energy Landscapes of Supramolecular Peptide-Drug Conjugates Directed by Linker Selection and Drug Topology. *Acs Nano* **2022,** *16* (6), 9546-9558.
6. Cheetham, A. G.; Zhang, P. C.; Lin, Y.-A.; Lock, L. L.; Cui, H. G., Supramolecular Nanostructures Formed by Anticancer Drug Assembly. *Journal of the American Chemical Society* **2013,** *135* (8), 2907-2910.
7. Su, H.; Wang, F.; Wang, Y.; Cheetham, A. G.; Cui, H., Macrocyclization of a Class of Camptothecin Analogues into Tubular Supramolecular Polymers. *Journal of the American Chemical Society* **2019,** *141* (43), 17107-17111.
8. Fleming, S.; Ulijn, R. V., Design of nanostructures based on aromatic peptide amphiphiles. *Chemical Society Reviews* **2014,** *43* (23), 8150-8177.
9. Wall, B. D.; Zacca, A. E.; Sanders, A. M.; Wilson, W. L.; Ferguson, A. L.; Tovar, J. D., Supramolecular Polymorphism: Tunable Electronic Interactions within pi-Conjugated Peptide Nanostructures Dictated by Primary Amino Acid Sequence. *Langmuir* **2014,** *30* (20), 5946-5956.
10. Xue, W. F.; Homans, S. W.; Radford, S. E., Systematic analysis of nucleation-dependent polymerization reveals new insights into the mechanism of amyloid self-assembly. *Proceedings of the National Academy of Sciences of the United States of America* **2008,** *105* (26), 8926-8931.
11. Crippa, M.; Perego, C.; de Marco, A. L.; Pavan, G. M., Molecular communications in complex systems of dynamic supramolecular polymers. *Nature Communications* **2022,** *13* (1).
12. Gardin, A.; Perego, C.; Doni, G.; Pavan, G. M., Classifying soft self-assembled materials via unsupervised machine learning of defects. *Communications Chemistry* **2022,** *5* (1).
13. Batra, R.; Loeffler, T. D.; Chan, H.; Srinivasan, S.; Cui, H.; Korendovych, I. V.; Nanda, V.; Palmer, L. C.; Solomon, L. A.; Fry, H. C.; Sankaranarayanan, S., Machine learning overcomes human bias in the discovery of self-assembling peptides. *Nat Chem* **2022**.
14. Webb, M. A.; Jackson, N. E.; Gil, P. S.; de Pablo, J. J., Targeted sequence design within the coarse-grained polymer genome. *Science Advances* **2020,** *6* (43).
15. Manandhar, A.; Kang, M.; Chakraborty, K.; Tang, P. K.; Loverde, S. M., Molecular simulations of peptide amphiphiles. *Organic & Biomolecular Chemistry* **2017,** *15* (38), 7993-8005.
16. Kang, M.; Zhang, P.; Cui, H.; Loverde, S. M., π–π Stacking Mediated Chirality in Functional Supramolecular Filaments. *Macromolecules* **2016,** *49* (3), 994-1001.
17. Manandhar, A.; Chakraborty, K.; Tang, P. K.; Kang, M.; Zhang, P. C.; Cui, H. G.; Loverde, S. M., Rational Coarse-Grained Molecular Dynamics Simulations of Supramolecular Anticancer Nanotubes. *Journal of Physical Chemistry B* **2019,** *123* (50), 10582-10593.
18. Mansbach, R. A.; Ferguson, A. L., Machine learning of single molecule free energy surfaces and the impact of chemistry and environment upon structure and dynamics. *Journal of Chemical Physics* **2015,** *142* (10).
19. Hamsici, S.; White, A. D.; Acar, H., Peptide framework for screening the effects of amino acids on assembly. *Science Advances* **2022,** *8* (3).
20. Laio, A.; Parrinello, M., Escaping free-energy minima. *Proc Natl Acad Sci U S A* **2002,** *99* (20), 12562-6.
21. Ianiro, A.; Wu, H. L.; van Rijt, M. M. J.; Vena, M. P.; Keizer, A. D. A.; Esteves, A. C. C.; Tuinier, R.; Friedrich, H.; Sommerdijk, N.; Patterson, J. P., Liquid-liquid phase separation during amphiphilic self-assembly. *Nature Chemistry* **2019,** *11* (4), 320-328.
22. Shimada, T.; Sakamoto, N.; Motokawa, R.; Koizumi, S.; Tirrell, M., Self-Assembly Process of Peptide Amphiphile Worm-Like Micelles. *Journal of Physical Chemistry B* **2012,** *116* (1), 240-243.
23. Jain, A.; Kassem, S.; Fisher, R. S.; Wang, B. R.; Li, T. D.; He, Y.; Elbaum-Garfinkle, S.; Ulijn, R. V.; Wang, T., Connected Peptide Modules Enable Controlled Co-Existence of Self-Assembled Fibers Inside Liquid Condensates. *Journal of the American Chemical Society* **2022,** *144* (33), 15002-15007.
24. Gao, X. Y.; Matsui, H., Peptide-based nanotubes and their applications in bionanotechnology. *Advanced Materials* **2005,** *17* (17), 2037-2050.

25. Eisele, D. M.; Cone, C. W.; Bloemsma, E. A.; Vlaming, S. M.; van der Kwaak, C. G. F.; Silbey, R. J.; Bawendi, M. G.; Knoester, J.; Rabe, J. P.; Vanden Bout, D. A., Utilizing redox-chemistry to elucidate the nature of exciton transitions in supramolecular dye nanotubes. *Nature Chemistry* **2012,** *4* (8), 655-662.
26. Pashuck, E. T.; Stupp, S. I., Direct Observation of Morphological Tranformation from Twisted Ribbons into Helical Ribbons. *Journal of the American Chemical Society* **2010,** *132* (26), 8819-+.
27. Korevaar, P. A.; George, S. J.; Markvoort, A. J.; Smulders, M. M. J.; Hilbers, P. A. J.; Schenning, A.; De Greef, T. F. A.; Meijer, E. W., Pathway complexity in supramolecular polymerization. *Nature* **2012,** *481* (7382), 492-U103.
28. Cheetham, A. G.; Lin, Y.-a.; Lin, R.; Cui, H., Molecular design and synthesis of self-assembling camptothecin drug amphiphiles. *Acta Pharmacologica Sinica* **2017,** *38* (6), 874-884.
29. Tang, P. K.; Manandhar, A.; Hu, W.; Kang, M.; Loverde, S. M., The interaction of supramolecular anticancer drug amphiphiles with phospholipid membranes. *Nanoscale advances* **2021,** *3* (2), 370-382.
30. Kang, M.; Cui, H.; Loverde, S. M., Coarse-grained molecular dynamics studies of the structure and stability of peptide-based drug amphiphile filaments. *Soft Matter* **2017,** *13* (42), 7721-7730.
31. Dellago, C.; Bolhuis, P. G.; Chandler, D., Efficient Transition Path Sampling: Application to Lennard-Jones Cluster Rearrangements. *J. Chem. Phys.* **1998,** *108*, 9236.
32. Dellago, C.; Bolhuis, P. G.; Holm, P. C.; Kremer, P. K., *Advanced Computer Simulation Approaches for Soft Matter Sciences III*. 2009; Vol. 221, p 167.
33. Schlick, T., Molecular Dynamics-Based Approaches for Enhanced Sampling of Long-Time, Large-Scale Conformational Changes in Biomolecules. *F1000 Bio. Rep.* **2009,** *1*, 51.
34. Van Erp, T. S.; Nicolis, G.; Maes, D., *Kinetics and Thermodynamics of Multi-step Nucleation and Self-Assembly in Nanoscale Materials*. 2012; Vol. 151, p 27.
35. Abrams, C.; Bussi, G., Enhanced sampling in molecular dynamics using metadynamics, replica-exchange, and temperature-acceleration. *Entropy* **2014,** *16* (1), 163-199.
36. Torrie, G. M.; Valleau, J. P., Monte Carlo Free Energy Estimates Using Non-Boltzmann Sampling: Application to the Sub-Critical Lennard-Jones Fluid. *Chem. Phys. Lett.* **1974,** *28*, 578.
37. Torrie, G. M.; Valleau, J. P., Nonphysical sampling distributions in Monte Carlo free-energy estimation: Umbrella sampling. *Journal of Computational Physics* **1977,** *23* (2), 187-199.
38. ten Wolde, P. R.; Frenkel, D., Enhancement of protein crystal nucleation by critical density fluctuations. *Science* **1997,** *277* (5334), 1975-8.
39. Van Erp, T. S.; Moroni, D.; Bolhuis, P. G., A Novel Path Sampling Method for the Calculation of Rate Constants. *J. Chem. Phys.* **2003,** *118*, 7762.
40. Moroni, D.; van Erp, T. S.; Bolhuis, P. G., Investigating Rare Events by Transition Interface Sampling. *Phys. A* **2004,** *340*, 395.
41. Allen, R. J.; Frenkel, D.; ten Wolde, P. R., Simulating Rare Events in Equilibrium or Nonequilibrium Stochastic Systems. *J. Chem. Phys.* **2006,** *124*, 024102.
42. Allen, R. J.; Valeriani, C.; Rein ten Wolde, P., Forward Flux Sampling for Rare Event Simulations. *J. Phys.: Condens. Matter* **2009,** *21*, 463102.
43. Laio, A.; Gervasio, F. L., Metadynamics: A Method to Simulate Rare Events and Reconstruct the Free Energy in Biophysics, Chemistry and Material Science. *Rep. Prog. Phys.* **2008,** *71*, 126601.
44. Barducci, A.; Bussi, G.; Parrinello, M., Well-tempered metadynamics: a smoothly converging and tunable free-energy method. *Phys Rev Lett* **2008,** *100* (2), 020603.
45. Tribello, G. A.; Giberti, F.; Sosso, G. C.; Salvalaglio, M.; Parrinello, M., Analyzing and Driving Cluster Formation in Atomistic Simulations. *J Chem Theory Comput* **2017,** *13* (3), 1317-1327.
46. Tribello, G. A.; Bonomi, M.; Branduardi, D.; Camilloni, C.; Bussi, G., PLUMED 2: New feathers for an old bird. *Computer Physics Communications* **2014,** *185* (2), 604-613.
47. Percec, V.; Wilson, D. A.; Leowanawat, P.; Wilson, C. J.; Hughes, A. D.; Kaucher, M. S.; Hammer, D. A.; Levine, D. H.; Kim, A. J.; Bates, F. S.; Davis, K. P.; Lodge, T. P.; Klein, M. L.; DeVane, R. H.; Aqad, E.; Rosen, B. M.; Argintaru, A. O.; Sienkowska, M. J.; Rissanen, K.; Nummelin, S.; Ropponen, J., Self-Assembly of Janus Dendrimers into Uniform Dendrimersomes and Other Complex Architectures. *Science* **2010,** *328* (5981), 1009.
48. Liu, G.; Wang, H.; Jiang, Y., Recrystallization and Micronization of Camptothecin by the Supercritical Antisolvent Process: Influence of Solvents. *Industrial & Engineering Chemistry Research* **2013,** *52* (43), 15049-15056.
49. Zhang, H.; Hollis, C. P.; Zhang, Q.; Li, T., Preparation and antitumor study of camptothecin nanocrystals. *Int J Pharm* **2011,** *415* (1-2), 293-300.
50. Balasubramanian, S.; Alderfer, J. L.; Staubinger, R. M., Solvent- and concentration-dependent molecular interactions of Taxol. *Journal of Pharmaceutical Sciences* **1994,** *83*, 1470-1476.
51. Mastropaolo, Crystal and molecular structure of paclitaxel. *Proc Natl Acad Sci USA* **1995,** *92*, 6920-6924.

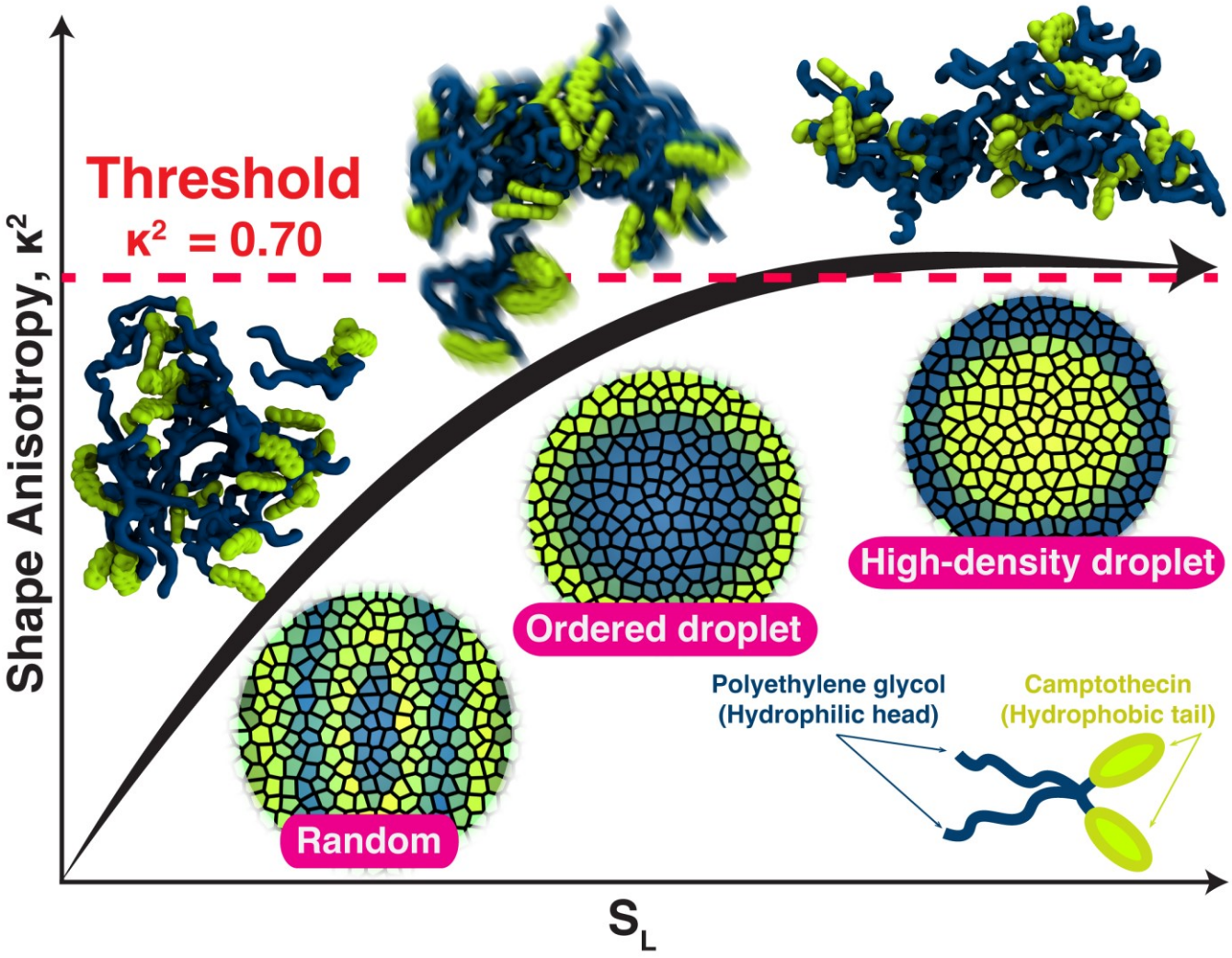
Threshold
κ² = 0.70
Shape Anisotropy, κ²
S_L
Random
Ordered droplet
High-density droplet
Polyethylene glycol
(Hydrophilic head)
Camptothecin
(Hydrophobic tail)